Check for updates

Received: 28 August 2025 | Revised: 12 October 2025 | Accepted: 6 February 2026

DOI: 10.1002/npp2.70038

ORIGINAL PAPER

New Plant Protection Open Access WILEY

Hyperspectral signatures reveal hidden stress in soybean caused by residual nicosulfuron

Shufei Hao[1] | Zekai Huang[1] | Olga A. Glazunova[2] | Konstantin V. Moiseenko[2] | Chi Wu[1] | Xingang Liu[1]

[1]State Key Laboratory for Biology of Plant Diseases and Insect Pests, Institute of Plant Protection, Chinese Academy of Agricultural Sciences, Beijing, China

[2]Russian State Agrarian University—Moscow Timiryazev Agricultural Academy, Moscow, Russia

Correspondence

Chi Wu and Xingang Liu.
Email: wuchi@caas.cn and liuxingangal@caas.cn

Funding information

National Key Research and Development Program of China, Grant/Award Numbers: 2023YFD1701300, 2024YFD1701101; Basic Research Center, Innovation Program of Chinese Academy of 24 Agricultural Sciences, Grant/Award Number: CAAS-BRC-GLCA-2025-01

Abstract

Residual nicosulfuron in soil can induce persistent phytotoxic effects on subsequent soybean (*Glycine max* L.) crops, yet the physiological trajectory from early stress to photosynthetic collapse remains unclear. Here, we established a multimodal phenotyping framework that integrates hyperspectral reflectance, ultraviolet-excited multichannel fluorescence, and chlorophyll fluorescence quenching imaging to capture stage-specific soybean responses under nicosulfuron stress. Early pigment disruption was marked by a 12.3% decrease in the chlorophyll index 3, while metabolic activation was indicated by an increase in fluorescence at 450 nm to 3.26 ± 0.16 at 100 μg/kg, compared to 2.05 ± 0.05 in the control group. These were followed by photosystem II (PSII) dysfunction, including a decline in the maximum quantum efficiency of PSII under light adaptation (Fv/Fm_Lss) from 0.71 to 0.37, a 102% increase in non-photochemical quenching under light adaptation (NPQ_Lss), and a 38% reduction in maximum fluorescence under light adaptation (Fm_Lss), reflecting photosystem disintegration. Such impairments culminated in a marked elevation of the Integrated Biomarker Response version 2. This study identifies a distinct injury–regulation–collapse pathway and phase-specific markers, while the integrated imaging approach enables earlier, non-invasive detection and dynamic monitoring, providing a mechanistic basis for risk assessment in herbicide-impacted rotation systems.

KEYWORDS

chlorophyll fluorescence, hidden stress detection, hyperspectral imaging, multi-modal phenotyping, residual nicosulfuron, soybean

1 | INTRODUCTION

In agricultural production, herbicides are vital strategic materials that guarantee food security and the quality of agricultural products.[1] Nevertheless, a substantial proportion of herbicides enter environmental media,[2] posing significant risks to environmental health, contaminating soils, and threatening the potential vitality of crops.[3,4] The extended application of long-residual herbicides depletes soil vitality and adversely impacts the growth and development of subsequent crops.[5,6] Additionally, herbicide residues in the soil can inflict phytotoxicity on subsequent crops.[7] Studies have confirmed that atrazine has caused notable phytotoxicity to subsequent soybeans,[8,9] and fluridone has significantly harmed subsequent maize crops.[10,11] The phytotoxicity of pesticides remaining in the soil to subsequent crops occurs frequently and warrants urgent attention.

This is an open access article under the terms of the Creative Commons Attribution License, which permits use, distribution and reproduction in any medium, provided the original work is properly cited.

© 2026 The Author(s). *New Plant Protection* published by John Wiley & Sons Australia, Ltd on behalf of Institute of Plant Protection, Chinese Academy of Agricultural Sciences.

Nicosulfuron, a widely employed herbicide by inhibiting acetolactate synthase (ALS),[12–14] offers advantages such as high efficacy at low application rates and is especially effective against grass weeds such as *Digitaria* and *Setaria* species in maize cultivation.[15] However, it poses notable risks to subsequent soybean crops due to its prolonged presence in the soil.[16] Research has shown that nicosulfuron residues in the soil can significantly affect subsequent soybean crops, particularly at higher concentrations. In studies conducted in northern China, concentrations exceeding 10 μg/kg were found to inhibit soybean germination and root development, leading to stunted growth and reduced yield.[17] Similarly, research in South America showed that concentrations up to 250 g a.i./ha caused visible injury to soybean plants, including decreased plant height and pod number.[18] Overall, the effect of nicosulfuron on soybeans is highly dependent on the residual concentration in the soil. Therefore, the safety concerns associated with the impact of nicosulfuron on the growth of subsequent soybean crops warrant significant attention.

Traditional assessments of herbicide phytotoxicity often rely on phenotypic observations such as growth suppression, leaf discoloration, or biomass reduction.[19–21] Though these methods are effective for confirming late-stage damage, they fail to detect subtle or early-stage impairments that may nonetheless have long-term impacts on crop productivity, and they provide little insight into the physiological mechanisms underlying toxicity. To address this gap, non-invasive imaging techniques have emerged as promising tools for capturing real-time physiological responses in plants.[22] In particular, hyperspectral reflectance, ultraviolet-excited multichannel fluorescence (UV-MCF), and chlorophyll fluorescence imaging have gained traction for their ability to monitor plant stress responses at multiple biological levels.[23–26] These techniques capture early pigment degradation, metabolic stress responses, and photosynthetic dysfunction, offering a multidimensional view of damage progression.[27] Compared to single-parameter measurements, this integrative imaging approach enhances both sensitivity and specificity in detecting early stress signatures, thus offering a powerful platform to assess complex, systemic responses—such as those elicited by nicosulfuron in soybean.

To address the current gap in understanding the physiological responses of soybean to nicosulfuron exposure, this study systematically investigated the progression from early, asymptomatic stages to overt phytotoxicity across a gradient of nicosulfuron concentrations. Specifically, this study aims to determine whether an integrative, multi-modal imaging app roach—combining hyperspectral reflectance, UV-MCF imaging, and chlorophyll fluorescence quenching analyses—can sensitively detect and characterize the early, hidden stress responses of soybean under residual nicosulfuron exposure. First, a controlled pot experiment was conducted to visually assess its pheno typic effects on soybean emergence, growth, and morphology, thereby characterizing the phenotypic responses at different stress levels. Second, to elucidate the potential toxic effects of nicosulfuron on the photosynthetic apparatus, an integrated imaging approach combining hyperspectral reflectance analysis, UV-MCF imaging, and chlorophyll fluorescence quenching imaging was employed. Hyperspectral reflectance imaging captures subtle variations in leaf optical properties across visible and near-infrared wavelengths, offering quantitative insights into pigment composition, tissue structure, and water status. UV-MCF imaging records fluorescence emissions related to metabolic activity and pigment stability, sensitively reflecting stress-induced biochemical changes. Chlorophyll fluorescence quenching analysis quantifies photochemical and non-photochemical energy dissipation processes, directly characterizing photosystem II (PSII) efficiency and photoprotective regulation. Each of these techniques targets a distinct physiological dimension—structural, metabolic, or photochemical, providing complementary information on different stages of the stress response. When integrated, they form a coherent framework that links early pigment perturbations with subsequent metabolic adjustments and photochemical dysfunction. This multimodal framework therefore enables a comprehensive assessment of changes in pigment composition, metabolic state, and PSII functionality, thereby characterizing the impairment patterns of photosynthetic performa nce at different stress stages. Finally, the Integrated Biomarker Response version 2 (IBRv2) was applied to synthesize multi-modal imaging parameters and identify early-stage phytotoxic biomarkers capable of sensitively indicating herbicide injury prior to the onset of visible symptoms.

Unlike conventional single-indicator analyses, this integrative framework allows for cross-validation among hyperspectral, fluorescence, and quenching parameters, linking structural, biochemical, and photochemical responses within a unified diagnostic system. This methodological integration enhances detection sensitivity and provides novel insights into the hidden progression of herbicide-induced stress that are difficult to capture using isolated approaches. Collectively, the results reveal the dynamic progression of nicosulfuron-induced damage in soybean, from metabolic adjustment to photosynthetic collapse, and establish a systematic diagnostic framework for early detection and risk assessment of residual herbicide stress, providing valuable implications for safe soybean cultivation and herbicide residue management. The demonstrated applicability of this multi-modal imaging framework

29949890, 2026, 1, Downloaded from https://onlinelibrary.wiley.com/doi/10.1002/npp2.70038 by CochraneChina, Wiley Online Library on [08/06/2026]. See the Terms and Conditions (https://onlinelibrary.wiley.com/terms-and-conditions) on Wiley Online Library for rules of use; OA articles are governed by the applicable Creative Commons License

provides a transferable basis for early stress diagnosis and precision management in other crop herbicide systems.

2 | MATERIALS AND METHODS

2.1 | Plant materials and chemicals

The soybean variety Zhonghuang 13 was supplied by Shouguang Taonong Agricultural Technology Co., Ltd. (Shouguang, China). Standard nicosulfuron (purity 98.4%) was obtained from Beijing Qincheng Yixin Technology Development Co., Ltd. (Beijing, China). Analytical-grade acetonitrile was obtained from Sinopharm Group Chemical Reagent Co., Ltd. (Shanghai, China). The experimental soil type was black soil from Jiaohe, Jilin Province, China. The physicochemical properties of the soil are provided in the Supporting Information (Supporting Information S1: Table S1). The other information involved in this paper can be obtained from Supporting Information S1.

2.2 | Phytotoxicity characterization

A pot experiment was conducted to evaluate the phytotoxicity of nicosulfuron on soybean seedlings. Nicosulfuron solutions were added to 500 ± 1 g of soil to achieve final concentrations of 0, 50, 100, 500 μg/kg, with thorough mixing. These concentrations were selected based on reported residue levels in post-maize cropping soils and prior assessments of herbicide-induced phytotoxicity in legumes.[17] Five seeds were planted per pot at a depth of 3 cm, with each treatment replicated three times. Seedlings were cultivated in incubators for 14 days under controlled conditions (14 h light/10 h dark, 25°C, 50% humidity, and 30% soil moisture).

Phytotoxicity symptoms were recorded after 14 days of cultivation. Plant height (measured from the stem base to the apical meristem) and primary root length were measured manually using a stainless-steel straightedge (±0.1 cm accuracy). Shoot fresh weight was determined with an analytical balance (±0.001 g). The seedling emergence rate was calculated as (emerged plants/sown seeds) × 100%. All measurements were conducted on five uniformly selected seedlings per pot, with three replicate pots per treatment.

2.3 | Determination of hyperspectral data

After 14 days of cultivation, hyperspectral imaging was conducted on soybean seedlings exposed to one control and three levels of nicosulfuron. For each concentration, three representative plants were gently removed from pots for imaging. The entire shoots (excluding roots) were stabilized in a neutral holder and scanned immediately for whole-plant physiological assessment. From these same plants, three fully expanded upper-canopy leaves (the 3rd–4th leaf from the apex) per replicate were selected, detached at the petiole, placed adaxial-side up on the imaging stage, and scanned for leaf-specific analysis. All scans were completed within 15 min of removal to minimize physiological changes.

Hyperspectral data were collected on the same leaves using a FluorTron multifunctional hyperspectral imaging system (Beijing Ecotech Science and Technology Ltd., Beijing, China) covering a spectral range of 400–1000 nm, with full-spectrum sunlight and UV light (up to 255 levels) as light sources, including both reflectance and UV-MCF information.

Plant spectral responses were captured using two complementary systems. Reflectance spectra across 400–1000 nm were acquired with a FluorTron® imaging system under simulated sunlight illumination at 255 UV intensity units. Concurrently, UV-MCF imaging employed a 365 nm UV-LED excitation source to induce both blue-green fluorescence emission (400–550 nm) and chlorophyll fluorescence (650–800 nm). Fluorescence emissions were recorded at four characteristic wavelengths: fluorescence at 450 nm (F450) and F542 (blue–green region), which are sensitive to pigment reorganization and mesophyll scattering; and F682 and F737 (red and far-red peaks), which reflect the photochemical activity of PSII and PSI, respectively. All measurements were performed at 14 days after the initiation treatment for all four concentration groups.

In addition, radar plots were used to visualize relative hyperspectral response patterns across treatments. For this purpose, each hyperspectral index (X_i) was expressed as a relative deviation from the control (X_{ck}) according to:

$$R_i = \frac{X_i - X_{ck}}{X_{ck}}$$

where X_i represents the index value under a given treatment and X_{ck} is the mean value of the control group. The resulting dimensionless values were used for radar plot construction to compare response profiles among treatments.

2.4 | Measurement of chlorophyll fluorescence parameters

Prior to measurement, selected leaves were dark-adapted for 20 min using specialized leaf clips. The FluorCam system (Closed FluorCam FC 800-C, Photon Systems Instruments, Brno, Czech Republic) with

29949890, 2026, 1, Downloaded from https://onlinelibrary.wiley.com/doi/10.1002/npp2.70038 by CochraneChina, Wiley Online Library on [08/06/2026]. See the Terms and Conditions (https://onlinelibrary.wiley.com/terms-and-conditions) on Wiley Online Library for rules of use; OA articles are governed by the applicable Creative Commons License

Quenching-Act2 protocol then applied sequential actinic light (1200 μmol photons·m^{-2} s^{-1} PAR) and saturating pulses (3000 μmol photons·m^{-2} s^{-1}, 800 ms duration) to quantify photosynthetic parameters. Steady-state photochemical quenching (QY_Lss) was calculated as (Fm' – Fs)/Fm' where Fm' represents maximum fluorescence under light adaptation and Fs denotes steady-state fluorescence. Concurrently, non-photochemical quenching (NPQ_Lss) was derived as (Fm – Fm')/Fm' according to the Loriaux standard formulation, with Fm indicating maximum dark-adapted fluorescence. All measurements were conducted on the same leaf positions previously subjected to hyperspectral analysis, and detailed definitions and explanations of all indices are provided in Supporting Information S1: Table S2.

2.5 | IBRv2 analysis with screened biomarkers

To integrate the results obtained from multiple imaging-based biomarkers and to understand the overall physiological responses of crops to herbicide exposure, IBRv2 was applied, following the methodology proposed by Sanchez et al.[28] IBRv2 is a modified version of the original IBR method developed by Beliaeff and Burgeot,[29] designed to quantify biological stress through a unified index. In this study, two independent sets of imaging data, hyperspectral imaging and chlorophyll fluorescence imaging were analyzed separately to extract a range of physiological and biochemical indicators reflecting herbicide-induced stress. These endpoints were then integrated into a single "stress index" to quantify the overall response at each treatment concentration, based on the principle of reference deviation.

Briefly, each individual biomarker value X_i (e.g., a spectral index from hyperspectral imaging or a fluorescence parameter from chlorophyll-fluorescence imaging) is first referenced to its control mean X_0 and subsequently logtransformed to reduce heteroscedasticity:

$$Y_i = \log\left(\frac{X_i}{X_0}\right)$$

Next, we compute the overall mean μ and standard deviation σ of the full set of Y_i values (across all concentrations and biomarkers), and standardize each observation:

$$Z_i = \frac{Y_i - \mu}{\sigma}$$

To center the control at zero and express deviations from baseline, we subtract the mean standardized control value Z_0 from each Z_i, yielding the biomarker deviation index A:

$$A = Z_i - Z_0$$

The IBRv2 was calculated as the sum of normalized deviations for all biomarkers (A_j), with equal weighting applied to each endpoint. The IBRv2 value is defined as follows:

$$\mathrm{IBRv2} = \Sigma_{j=1}^{n} |A_j|$$

The IBRv2 method applies equal weighting to integrate structural, physiological, and biochemical plant indicators, avoiding subjective bias from manual weighting. This approach enhances objectivity and applicability, simplifies procedures, and works reliably across diverse environmental and data conditions without relying on prior assumptions, aligning with the complex realities of ecological research.

2.6 | Statistical analyses

All data are presented as means ± standard deviations (SD) from three independent biological replicates ($n = 3$). Prior to analyses, data were tested for normality using the Shapiro–Wilk test and for homogeneity of variance using Bartlett's test. When the assumptions were satisfied, differences were evaluated with Student's *t*-test. Statistical analyses were conducted in GraphPad Prism 9.5.1 (GraphPad Software, San Diego, CA, USA), with a significance level set at 0.05. Significance levels were denoted in figures as follows: *$p < 0.05$, **$p < 0.01$, ***$p < 0.001$, ****$p < 0.0001$, and "ns" for non-significant differences. Spectral data processing, including reflectance curves, spectral derivatives, and pseudocolor imaging, was conducted using OriginPro 2022 (OriginLab Corporation, Northampton, MA, USA).

3 | RESULTS

3.1 | Effects of nicosulfuron treatment on the growth of soybean seedlings

Exposure to increasing concentrations of nicosulfuron induced visible and statistically significant phytotoxic effects in soybean seedlings, as reflected by reduced emergence, impaired early growth, and altered shoot and root morphology (Figure 1A–E). Among these, seedling emergence rate was the earliest and most sensitive indicator of stress (Figure 1B). At 50 μg/kg, emergence rates remained relatively unaffected (86.9% ± 6.2%). However, the rates declined sharply at higher concentrations, falling to 78.1% ± 9.0% at 100 μg/kg ($p < 0.01$) and 55.9% ± 10.2% at 500 μg/kg ($p < 0.0001$), indicating severe interference with germination and early seedling establishment. Following the

29949890, 2026, 1, Downloaded from https://onlinelibrary.wiley.com/doi/10.1002/npp2.70038 by CochraneChina, Wiley Online Library on [08/06/2026]. See the Terms and Conditions (https://onlinelibrary.wiley.com/terms-and-conditions) on Wiley Online Library for rules of use; OA articles are governed by the applicable Creative Commons License

suppression of emergence, soybean seedling growth exhibited the clear, concentration-dependent inhibition. Plant height declined significantly to 34.17 ± 0.62 cm, 27.83 ± 0.85 cm, and 21.67 ± 1.25 cm at concentrations of 50, 100, and 500 μg/kg (Figure 1C), respectively, compared to 37.50 ± 1.08 cm in the control group (CK) ($p < 0.05$), indicating a progressive reduction in shoot elongation under increasing herbicide stress. Primary root length also exhibited pronounced sensitivity to nicosulfuron (Figure 1D). No significant change was detected at 50 μg/kg, but a marked reduction occurred at higher concentrations, with root length decreasing to 9.16 ± 0.74 cm at 500 μg/kg, compared to 18.50 ± 1.08 cm in CK ($p < 0.0001$), representing a reduction exceeding 50%. This sharper decrease may indicate a higher sensitivity of root growth to soil-borne exposure. Fresh weight was further analyzed to assess overall seedling growth. Fresh weight also declined with increasing concentrations (Figure 1E). No significant change was observed at 50 μg/kg, but at 100 and 500 μg/kg, biomass dropped significantly, reaching a minimum of 1.8 ± 0.2 g under the highest dose ($p < 0.001$).

3.2 | Hyperspectral reflectance analysis

Following the morphological suppression effects, hyperspectral reflectance imaging provided a sensitive and non-destructive means to assess early physiological disturbances. As a composite indicator of cumulative stress signals, the integrated index IBRv2 increased across all treatments, reaching 14.53, 24.51, and 27.25 under 50, 100, and 500 μg/kg exposures, respectively (Figure 2A). Notably, at 50 μg/kg, the index was already higher than that in the control, suggesting an early onset of physiological disturbance and the initiation of stress responses. Consistent with the integrated index, reflectance at 542 nm, a chlorophyll absorption-sensitive band, exhibited a clear concentration-dependent increase (Figure 2B). Under control conditions, reflectance at this wavelength remained low (0.11 ± 0.01), whereas progressively higher reflectance values were observed with increasing residue levels, reaching approximately 0.13 at 500 μg/kg, reflecting a gradual disturbance in chlorophyll absorption and mesophyll structural integrity.

To facilitate the interpretation of the radar plot-based responses, hyperspectral indices were grouped according to their primary physiological relevance (Figure 2C–F). Indices related to pigment content and canopy structure or vitality, such as normalized difference vegetation index (NDVI), NIRv, chlorophyll index 1–4 (CHL1–CHL4), red edge NDVI (RENDVI), modified red edge normalized difference vegetation index (MRENDVI), and modified triangular vegetation index (MTVI), primarily describe chlorophyll abundance, red-edge position, and overall canopy photosynthetic vigor. Pigment absorption and red-edge structural indices, including modified chlorophyll absorption ratio

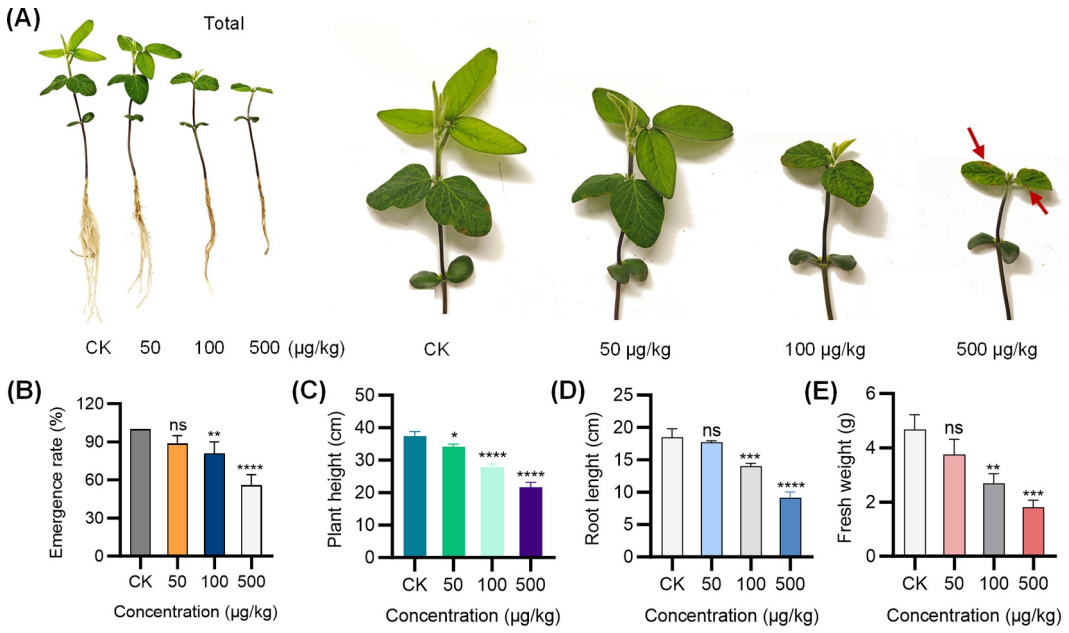

FIGURE 1 Effects of nicosulfuron at different concentrations on plant growth parameters. (A) Representative soybean seedlings after 14 days of cultivation under four nicosulfuron concentrations (0, 50, 100, and 500 μg/kg). Red arrows indicate leaf chlorosis and deformation at high concentration. (B–E) Quantitative analysis of seedling traits including emergence rate (B), plant height (C), root length (D) and fresh weight (E). Error bars represent means ± SD ($n = 3$). ns: not significant; Asterisks indicate statistically significant differences (*$p < 0.05$, **$p < 0.01$, ***$p < 0.001$, ****$p < 0.0001$).

29949890, 2026, 1, Downloaded from https://onlinelibrary.wiley.com/doi/10.1002/npp2.70038 by CochraneChina, Wiley Online Library on [08/06/2026]. See the Terms and Conditions (https://onlinelibrary.wiley.com/terms-and-conditions) on Wiley Online Library for rules of use; OA articles are governed by the applicable Creative Commons License

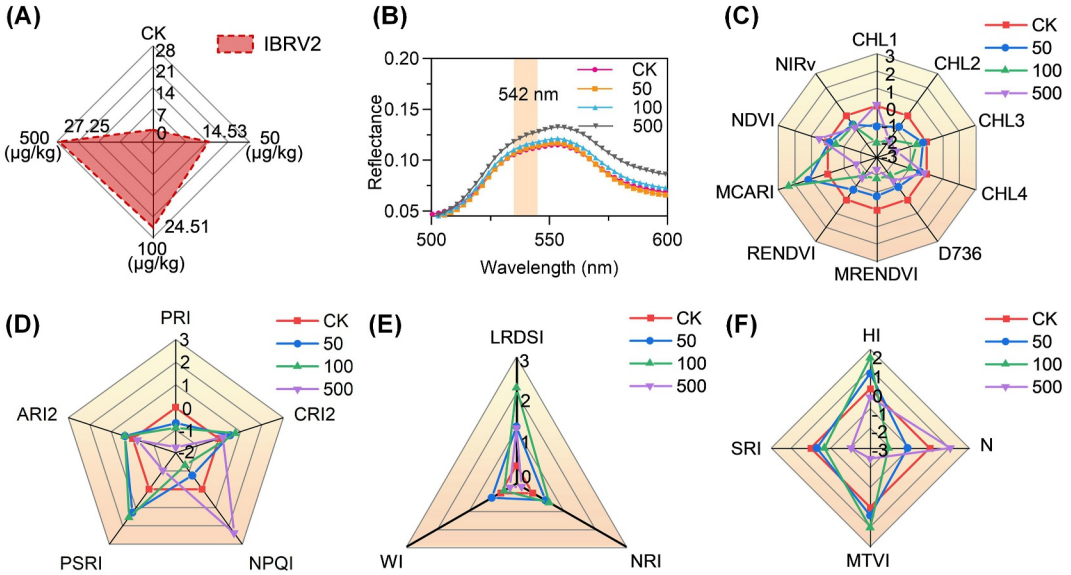

FIGURE 2 Hyperspectral reflectance-based assessment of soybean responses to residual nicosulfuron exposure. (A) Integrated Biomarker Response version 2 (IBRv2) scores under 50, 100, and 500 μg/kg treatments, indicating increasing stress with higher herbicide concentrations. (B) Mean reflectance spectra in the 500–600 nm range, showing a prominent peak at 542 nm and a concentration-dependent rise in reflectance intensity. (C–F) Z-score radar plots of hyperspectral indices under 0, 50, 100, and 500 μg/kg, categorized into pigment and canopy structure (NDVI, CHL1–CHL4, MCARI, D736) (C), pigment composition and stress (PRI, ARI2, CRI2, PSRI, NPQI) (D), water and light response (WI, NRI, LRDSI) (E), and vitality/nitrogen-related metrics (HI, SRI, N, MTVI) (F). Dose-dependent shifts in multiple spectral indices indicate coordinated alterations in multiple spectral indices associated with pigment status and canopy structure. ARI2, anthocyanin reflectance index 2; CHL, chlorophyll index; CRI2, carotenoid reflectance index 2; D736, first-derivative reflectance at 736 nm; HI, health index; LRDSI, leaf red-edge drought stress index; MCARI, modified chlorophyll absorption ratio index; MTVI, modified triangular vegetation index; N, nitrogen index; NDVI, normalized difference vegetation index; NPQI, normalized phaeophytinization index; NRI, nitrogen reflectance index; PRI, photochemical reflectance index; PSRI, plant senescence reflectance index; SRI, simple ratio index; WI, water index.

index (MCARI) and first-derivative reflectance (D736), are particularly sensitive to chlorophyll absorption characteristics and changes in red-edge spectral shape. Photochemical regulation and pigment composition, as well as stress-related indices, including the photochemical reflectance index (PRI), normalized phaeophytinization index (NPQI), plant senescence reflectance index (PSRI), anthocyanin reflectance index 2 (ARI2), and carotenoid reflectance index 2 (CRI2), reflect light-use efficiency, energy dissipation, chlorophyll integrity, and shifts in accessory pigments. Water and light-response indices, such as water index (WI), nitrogen reflectance index (NRI), and leaf red-edge drought stress index (LRDSI), provide complementary information on leaf water status and light-response behavior, whereas nutrient and vitality related indices, such as nitrogen index (N), simple ratio index (SRI), and health index (HI), describe nitrogen associated reflectance features and overall plant health. In addition, the carotenoid-related red-edge index (CARrededge) was included in the pseudocolor visualization to illustrate stress-related changes in red-edge spectral features associated with carotenoid dynamics.

At 50 μg/kg, the radar plot showed only mild overall displacement, with pronounced changes confined to a limited number of sensitive indices (Figure 2C–F). Specifically, NDVI and CHL3–CHL4 did not exhibit obvious displacement at this dose, and their raw values did not differ significantly from the control, indicating that canopy pigment content and structural characteristics remained largely stable (Figure 2C). In contrast, several stress and energy regulation related indices showed early responses: PSRI and MCARI displayed slight outward shifts, while the red edge related index D736 and CHL1 declined, suggesting that canopy spectral properties had begun to respond to residual stress even in the absence of visible morphological symptoms.

At 100 μg/kg, the radar plot revealed a pronounced overall displacement across most indices, indicating a more intensive and coordinated alteration of spectral and fluorescence responses at this intermediate residue level (Figure 2C–F). Among these responses, MCARI exhibited a pronounced upward displacement. For example, its value increased from 0.15 ± 0.02 in the control to 0.23 ± 0.03 at 100 μg/kg ($p < 0.0001$; Supporting Information S1: Figure S1A). Concurrently, a broad shift was observed across multiple chlorophyll associated indices and red edge metrics, with the RENDVI and D736 showing a significant reduction and chlorophyll related indices (CHL1–CHL4) continued to

29949890, 2026, 1, Downloaded from https://onlinelibrary.wiley.com/doi/10.1002/npp2.70038 by CochraneChina, Wiley Online Library on [08/06/2026]. See the Terms and Conditions (https://onlinelibrary.wiley.com/terms-and-conditions) on Wiley Online Library for rules of use; OA articles are governed by the applicable Creative Commons License

decline, extending the downward trend already observed at 50 μg/kg. Within the photochemical regulation and pigment composition related indices, NPQI showed a pronounced decline at 100 μg/kg, decreasing from 0.041 ± 0.002 in the control to 0.018 ± 0.001 ($p < 0.0001$), corresponding to a reduction of approximately 55% (Figure 2D, Supporting Information S1: Figure S1B). Within the water and light response related indices, LRDSI exhibited the most pronounced expansion in the radar plot at 100 μg/kg, reaching a peak value of 13.84 ± 1.07 ($p < 0.0001$; Figure 2E and Supporting Information S1: Figure S1C). Whereas nutrient and vitality related indices, including N and HI, also continued to change along the dose gradient.

At 500 μg/kg, index responses deviated from the previously coupled dose-dependent pattern and displayed increased heterogeneity across groups. Within the pigment and canopy structure related indices (Figure 2C), an overall declining trend was observed; however, several indices, including CHL1, CHL4, MCARI, and NDVI, exhibited rebound responses relative to the mid dose level. Among the stress and regulation related indices (Figure 2D), most indices showed pronounced contraction. Notably, NPQI declined from 0.041 ± 0.002 in the control to 0.018 ± 0.001 at 100 μg/kg but then increased sharply to 0.075 ± 0.001 at 500 μg/kg ($p < 0.0001$; Supporting Information S1: Figure S1B), meanwhile, CRI2 also increased relative to its value at 100 μg/kg. In the water and light response group (Figure 2E), LRDSI showed a rebound, whereas the remaining indices continued to decline. In contrast, all nutrient and vitality related indices (Figure 2F) underwent marked contraction at this concentration.

Hyperspectral pseudocolor maps provided a direct spatial representation of canopy spectral responses under different residue levels (Figure 3). In the control treatment, most indices exhibited spatially continuous distributions with relatively uniform high-value patterns across the canopy, although index specific structural features were already observable in some maps. At 50 μg/kg, spatial patterns remained largely comparable to the control. NDVI and PRI maps were still dominated by relatively high-value regions, while CHL4 exhibited an overall downward shift in signal intensity accompanied by enhanced internal structural contrast rather than the formation of distinct localized patches. At 100 μg/kg, spatial differentiation became more apparent, with low-value regions expanding in extent and contrast across the canopy, a response that was more clearly expressed in the CHL4 and PRI maps. At 500 μg/kg, spatial contrast became more pronounced. In the NDVI maps (Figure 3C), large contiguous areas with intermediate to relatively high values were still preserved, while low-value regions appeared more frequently, indicating reduced spatial uniformity without complete loss of canopy coverage. In contrast, the CHL4 and PRI maps (Figure 3D,F) showed a broader distribution of lower signal intensities across leaf areas, reflecting a stronger spatial response relative to lower concentrations.

3.3 | UV-MCF fluorescence analysis

To further elucidate the physiological responses of soybean seedlings to nicosulfuron stress, UV-MCF imaging was employed to quantify both the absolute intensity and ratio indices across four key channels (F450, F542, F682, and F737) (Figure 4A–D), capturing the entire stress trajectory from early metabolic responses to photochemical system collapse.

UV-MCF fluorescence measurements revealed concentration-dependent changes across all four emission channels (Figure 4A–D). F450 and F542 increased markedly from control levels and reached their maxima at 100 μg/kg, with F450 rising from 2.05 to 3.26 ($p < 0.0001$) and F542 from 1.30 to 2.03 ($p < 0.0001$). Both channels showed a slight decline at 500 μg/kg. In contrast, the chlorophyll-related emissions exhibited a different trend: F682 remained close to control levels at lower concentrations but declined sharply at 500 μg/kg, and F737 correspondingly decreased with increasing concentrations. Relative to the control, F682 decreased by 15.5%, whereas F737 showed a more pronounced reduction of 27.1% ($p < 0.0001$), indicating a stronger suppression of far-red chlorophyll fluorescence under high residual stress. At higher exposure levels, the reduction in F737 was more pronounced than that observed for F682, indicating a divergence between the two chlorophyll-associated channels under higher exposure.

To clarify how residual nicosulfuron altered the relative balance among chlorophyll-associated and short-wavelength fluorescence emissions, three complementary fluorescence ratios (F682/F737, F450/F737, and F450/F682) were analyzed (Supporting Information S1: Figure S2). Compared with the control (1.716 ± 0.018), F682/F737 decreased to 1.536 ± 0.014 at 50 μg/kg ($p < 0.05$), 1.374 ± 0.014 at 100 μg/kg ($p < 0.0001$), and 1.325 ± 0.013 at 500 μg/kg ($p < 0.01$) (Supporting Information S1: Figure S2A). Correspondingly, F450/F737 increased significantly at 100 μg/kg, reaching 1.22 compared with 1.04 in the control ($p < 0.01$), before returning to control levels at 500 μg/kg, with a value of 1.03 and no significant difference (Supporting Information S1: Figure S2B). In contrast, F450/F682 remained relatively stable at lower concentrations, with a significant decrease observed only at 500 μg/kg, declining from 4.56 in the control to 3.20 ($p < 0.01$) (Supporting Information S1: Figure S2C). These ratio changes reflect shifts in the relative intensities of short-wavelength and

29949890, 2026, 1, Downloaded from https://onlinelibrary.wiley.com/doi/10.1002/npp2.70038 by CochraneChina, Wiley Online Library on [08/06/2026]. See the Terms and Conditions (https://onlinelibrary.wiley.com/terms-and-conditions) on Wiley Online Library for rules of use; OA articles are governed by the applicable Creative Commons License

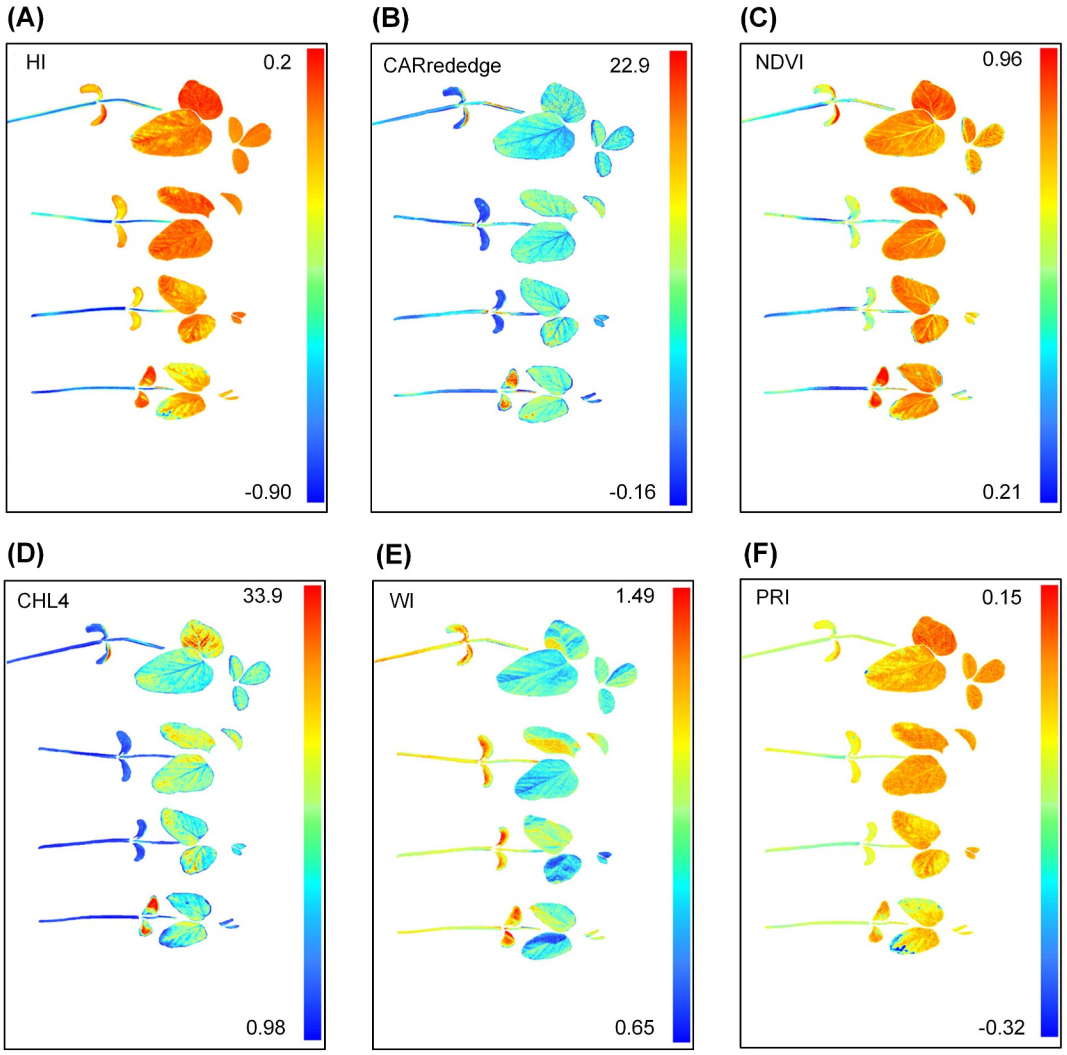

FIGURE 3 Hyperspectral pseudocolor images of soybean seedlings under different nicosulfuron concentrations. (A) HI, reflecting overall pigment composition; (B) CARrededge, reflecting changes in red-edge spectral characteristics associated with carotenoid-related signals; (C) NDVI, representing leaf greenness and photosynthetic activity; (D) CHL4, estimating relative chlorophyll concentration; (E) WI, associated with leaf water content; and (F) PRI, related to light-use efficiency of photosynthesis. Each column from top to bottom corresponds to increasing nicosulfuron concentrations: 0, 50, 100, and 500 μg/kg. Color scales represent relative index values, with red denoting higher values and blue indicating lower values. CARrededge, carotenoid-related red-edge index; CHL4, chlorophyll index 4; HI, health index; NDVI, normalized difference vegetation index; PRI, photochemical reflectance index; WI, water index.

chlorophyll-associated fluorescence under increasing exposure.

Fluorescence pseudocolor maps (Figure 4E) were consistent with the quantitative intensity results and showed broadly comparable spatial patterns across the leaf surface, with treatment-dependent differences in overall signal intensity. At 100 μg/kg, F450 and F542 exhibited an overall enhancement in fluorescence signal across the leaf, in line with the increased mean intensities observed in the numerical analysis. At 500 μg/kg, fluorescence intensity declined across all channels, particularly for the chlorophyll related emissions, reflecting the strong suppression detected in the corresponding intensity measurements. Together, the pseudocolor maps provide spatial context for the intensity-based analyses and indicate that nicosulfuron induced fluorescence responses were expressed primarily as changes in overall emission level.

3.4 | Changes in chlorophyll fluorescence quenching under nicosulfuron stress

Building on the previous analyses, this section further explores the functional changes in the photosynthetic machinery of soybean under nicosulfuron stress through chlorophyll fluorescence quenching parameters.

Nicosulfuron treatment induced a concentration-dependent disruption of the photosynthetic machinery,

29949890, 2026, 1, Downloaded from https://onlinelibrary.wiley.com/doi/10.1002/npp2.70038 by CochraneChina, Wiley Online Library on [08/06/2026]. See the Terms and Conditions (https://onlinelibrary.wiley.com/terms-and-conditions) on Wiley Online Library for rules of use; OA articles are governed by the applicable Creative Commons License

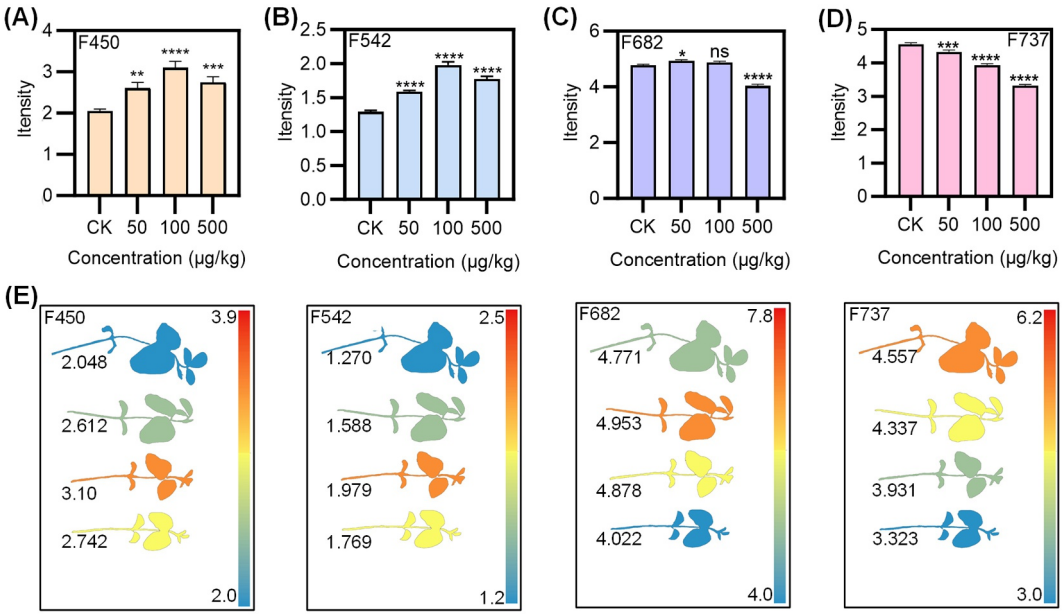

FIGURE 4 UV-excited multichannel fluorescence responses patterns in soybean leaves under different concentrations of nicosulfuron exposure using UV-induced chlorophyll fluorescence imaging. (A–D) The absolute fluorescence intensities of F450, F542, F682, and F737 channels. (E) Pseudocolor fluorescence images of the four channels (F450, F542, F682, F737), from top to bottom corresponding to CK, 50, 100, and 500 μg/kg treatments, showing the spatial distribution of fluorescence signals under different treatments.

beginning with structural impairment of PSII. The maximum fluorescence under light adaptation (Fm_Lss) (Figure 5A) declined significantly to 297.49 ± 6.80 at 500 μg/kg, compared to 476.32 ± 13.23 in the control, representing a 37.6% reduction ($p < 0.001$), indicating damage to the PSII reaction centers, which are known to be susceptible to sulfonylurea induced oxidative stress. The maximum quantum efficiency of PSII under light adaptation (Fv/Fm_Lss) (Figure 5B), representing the maximum quantum efficiency of PSII photochemistry, decreased moderately to 0.37, compared to 0.71 in the control ($p < 0.001$), further confirming functional impairment of the electron transport chain. The steady-state fluorescence decline ratio (Rfd_Lss) (Figure 5C), an indicator of plant vitality and carbon assimilation efficiency, showed a non-linear trend. It increased to 2.42 at 100 μg/kg, compared to 1.34 in the control ($p < 0.001$). In contrast, at 500 μg/kg, Rfd_Lss declined significantly to 2.00 ($p < 0.001$), although it remained higher than the control level. Overall, Rfd_Lss showed an initial increase at moderate exposure followed by a significant reduction at the highest concentration. Energy-related fluorescence parameters responded differently to increasing nicosulfuron concentrations (Figure 5D–F). Non-photochemical quenching under light adaptation (NPQ_Lss) increased from 0.826 ± 0.138 in the control to 1.194 ± 0.080 at 50 μg/kg ($p < 0.05$) and further to 1.671 ± 0.062 at 100 μg/kg ($p < 0.001$), before declining to 1.332 ± 0.111 at 500 μg/kg ($p < 0.01$; Figure 5D). In contrast, the photochemical quenching coefficient (qP_Lss) and the effective quantum yield of PSII photochemistry (QY_Lss) showed modest increases at higher concentrations (Figure 5E–F). Notably, at 500 μg/kg, increases in qP_Lss and QY_Lss occurred concurrently with significant reductions in Fm_Lss and Fv/Fm_Lss, indicating a divergence in the response patterns among fluorescence parameters at high exposure levels. This increase should be interpreted as a relative effect rather than evidence of functional recovery.

The cumulative disturbance was quantitatively evaluated using the IBRv2 (Figure 5G). This index increased from 0.79 at 50 μg/kg to 2.65 at 100 μg/kg and rose sharply to 11.10 at 500 μg/kg. The steep increase in IBRv2 at 500 μg/kg reflects a marked amplification of the overall deviation from the control.

4 | DISCUSSION

4.1 | Lagged growth responses and the necessity for functional optical assessment under residual nicosulfuron stress

In rotational cropping systems, residual ALS-inhibiting herbicides such as nicosulfuron frequently cause phytotoxicity in sensitive subsequent crops, with soybean being one of the species most vulnerable to carryover effects. In practice, the diagnosis of such injury largely relies on growth-based endpoints, including reductions in plant height, biomass, and root development, as these parameters directly reflect agronomic

29949890, 2026, 1, Downloaded from https://onlinelibrary.wiley.com/doi/10.1002/npp2.70038 by CochraneChina, Wiley Online Library on [08/06/2026]. See the Terms and Conditions (https://onlinelibrary.wiley.com/terms-and-conditions) on Wiley Online Library for rules of use; OA articles are governed by the applicable Creative Commons License

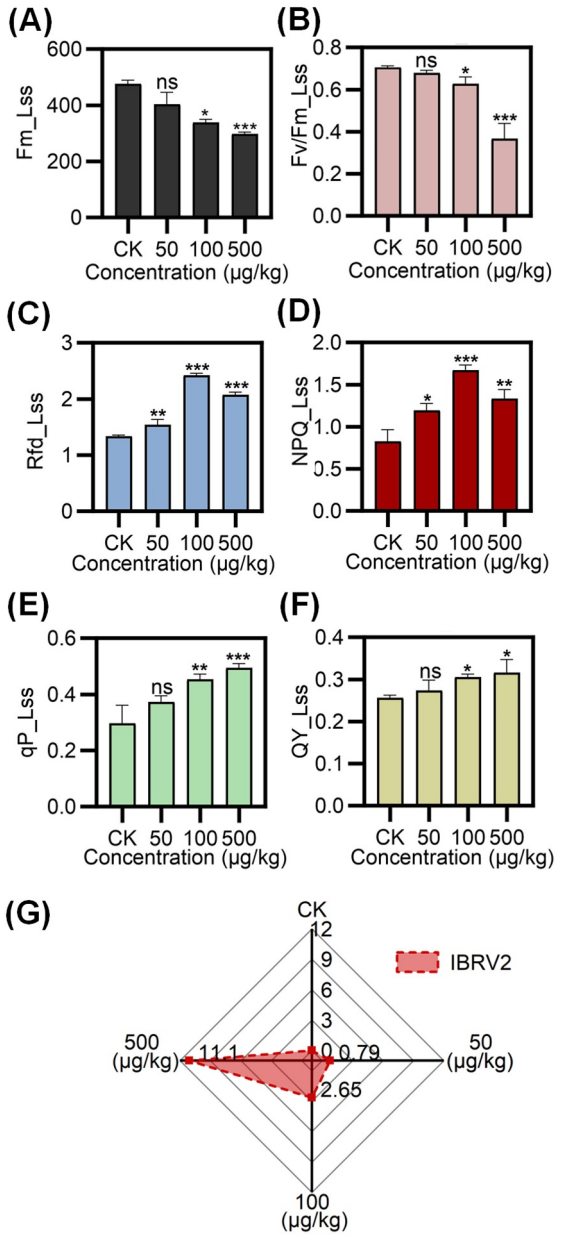

FIGURE 5 Phytotoxic effects of increasing concentrations of nicosulfuron on soybean, assessed through multiple chlorophyll fluorescence parameters. (A) Fm_Lss, (B) Fv/Fm_Lss, (C) Rfd_Lss, (D) NPQ_Lss, (E) qP_Lss, and (F) QY_Lss values under different nicosulfuron concentrations (0, 50, 100, 500 μg/kg). Significant differences are indicated by asterisks (*$p < 0.05$, **$p < 0.01$, ***$p < 0.001$). (G) Radar chart illustrating IBRv2 values across treatments. Fm_Lss, maximum fluorescence yield under light steady-state conditions; Fv/Fm_Lss, maximum quantum efficiency of PSII photochemistry under light steady-state conditions; IBRv2, Integrated Biomarker Response version 2; NPQ_Lss, non-photochemical quenching under light steady-state conditions; ns, not significant; qP_Lss, photochemical quenching coefficient under light steady-state conditions; QY_Lss, effective quantum yield of PSII photochemistry under light steady-state conditions; Rfd_Lss, steady-state fluorescence decline ratio (photosynthetic vitality index).

performance.[30] However, growth suppression represents a relatively late manifestation of stress, and by the time it becomes evident, physiological impairment has already progressed (Figure 1A–E). This limitation is particularly relevant under low to moderate residue levels, where plants may establish normally while subtle functional costs accumulate. Against this background, the present study focuses on coordinated shifts across multiple optical traits, using their joint responses to track the progressive impairment of photosynthetic and metabolic function before growth inhibition becomes apparent.

4.2 | Early functional changes revealed by hyperspectral and UV-MCF signals

At low residual levels of nicosulfuron, soybean seedlings exhibited only limited morphological impairment, indicating that the early responses were dominated by functional disturbances rather than generalized physiological impairments. At a concentration of 50 μg/kg, plant height showed a slight but significant reduction (Figure 1A), whereas fresh weight and root length remained largely unaffected. In contrast, hyperspectral analysis revealed an early increase in the integrated stress index IBRv2 (Figure 2A), together with significant increases in PSRI and MCARI, and a reduction in the red edge parameter D736 (Figure 2C). These responses indicate that pigment related optical properties and canopy structure were already affected before pronounced growth suppression occurred. In previous studies, changes in PSRI, MCARI, and red-edge related indices have been widely interpreted as early functional responses to sublethal chemical or environmental stress.[31–33] Rather than reflecting irreversible damage, such shifts are generally associated with initial pigment imbalances, altered light absorption, and subtle structural adjustments within the mesophyll.[34,35] The appearance of these signals at low residue levels in the present study is therefore consistent with reported early-stage stress responses induced by non-photosynthetic herbicides.

UV-MCF fluorescence provided complementary insights into these early functional alterations. Although the absolute chlorophyll-related fluorescence intensities (F682 and F737) remained close to control levels at 50 μg/kg, the ratio F682/F737 decreased significantly (Supporting Information S1: Figure S2A), indicating an early imbalance between PSII and PSI-associated fluorescence emissions.[36] Similar ratio shifts have been reported as sensitive indicators of excitation energy redistribution under mild stress, preceding broader changes in photosystem performance.[37] In contrast, ratios involving short-wavelength

29949890, 2026, 1, Downloaded from https://onlinelibrary.wiley.com/doi/10.1002/npp2.70038 by CochraneChina, Wiley Online Library on [08/06/2026]. See the Terms and Conditions (https://onlinelibrary.wiley.com/terms-and-conditions) on Wiley Online Library for rules of use; OA articles are governed by the applicable Creative Commons License

fluorescence showed only limited variation at this stage, suggesting that fluorescence reorganization was still incomplete.

Taken together, these observations indicate that residual nicosulfuron induces selective optical alterations at an early exposure stage. Early responses are confined to pigment- and structure-related hyperspectral indices, along with a specific shift in the PSII/PSI fluorescence balance. This defines an initial functional disturbance phase that precedes the more extensive photosynthetic regulation and growth inhibition observed at higher residue levels.

4.3 | Compensatory photosynthetic regulation at moderate residue levels

At a moderate residue level of 100 μg/kg, soybean seedlings exhibited coordinated changes across hyperspectral, UV-MCF, and chlorophyll fluorescence parameters, indicating an active regulatory response of the photosynthetic system rather than an immediate functional collapse. At this concentration, reductions in emergence rate, plant height, and fresh weight were already significant (Figure 1B,D–E), yet optical indicators suggested that the photosynthetic apparatus remained functionally engaged. This dissociation between growth inhibition and photosynthetic activity is a feature commonly reported under sublethal chemical stress, where regulation is intensified to sustain metabolic function despite declining growth performance.[38,39] Hyperspectral reflectance analysis revealed that pigment and photosynthesis related indices were broadly affected at 100 μg/kg. The sharp increase in MCARI, together with significant declines in PRI and CHL4 (Figure 2C; Supporting Information S1: Figure S1A, G, M), indicates altered chlorophyll absorption characteristics and reduced photosynthetic light use efficiency.[40,41] Similar combinations of MCARI elevation and PRI reduction have been reported under herbicide and nutrient stress and are often interpreted as signatures of increased excitation pressure and enhanced energy dissipation requirements.[42,43] At the same time, the continued decline in red edge parameters such as RENDVI and D736 suggests the progressive disruption of canopy optical structure and mesophyll organization, consistent with stress levels that exceed simple pigment adjustment.[44]

The UV-MCF fluorescence responses further clarify the regulatory nature of this concentration. Short-wavelength fluorescence emissions (F450 and F542) increased markedly and reached their maximum values at 100 μg/kg (Figure 4A,B), while chlorophyll-related emissions (F682 and F737) remained close to control levels. In previous studies, enhanced blue–green fluorescence has been associated with increased accumulation of stress-related fluorophores and elevated metabolic activity,[45] rather than with direct loss of chlorophyll function. Correspondingly, the significant increase in the F450/F737 ratio (Supporting Information S1: Figure S2B), together with the continued decline in the F682/F737 ratio (Supporting Information S1: Figure S2A), indicates a redistribution of fluorescence emission towards non-chlorophyll components and a persistent imbalance between PSII and PSI-associated emissions, a pattern widely interpreted as a regulatory adjustment under moderate stress.[30]

Chlorophyll fluorescence quenching parameters provide direct evidence that photoprotective regulation was actively engaged at this moderate concentration. The substantial increase in NPQ_Lss reflects enhanced non-photochemical energy dissipation (Figure 5D), a mechanism commonly activated to prevent photodamage when excitation energy exceeds photochemical capacity.[46] Similar Rfd increases (Figure 5C) under moderate stress have been reported previously and are generally interpreted as reflecting enhanced photosynthetic turnover rather than improved growth performance.[47] Importantly, Fm_Lss (Figure 5A) and Fv/Fm_Lss (Figure 5B) showed only moderate reductions at a residual concentration of 100 μg/kg, suggesting that PSII reaction centers were still largely intact and that regulatory adjustment, rather than structural damage, dominated the photosynthetic response at this stage.

Taken together, the optical responses observed at 100 μg/kg indicate a compensatory regulatory phase in which multiple regulatory pathways are activated simultaneously. In contrast to the selective optical deviations observed at low residue levels, this stage is characterized by a broader involvement of pigment, fluorescence, and energy dissipation parameters. Additionally, the preservation of PSII maximum efficiency distinguishes this phase from the functional decline observed at the highest residue level. These features indicate that moderate residual nicosulfuron exposure places soybean seedlings in a regulation-dominated state, where photosynthetic control mechanisms are intensified to buffer against increasing stress, albeit at the cost of growth performance.

4.4 | Transition from regulation to functional decline at high residue levels

At the highest residual level of nicosulfuron (500 μg/kg), the optical response pattern of soybean seedlings diverged fundamentally from that observed at low and moderate concentrations, indicating a shift from regulation-dominated responses to functional decline (Figure 1B–E). Previous studies on non-photosynthetic target herbicides and severe environmental stress have shown that when plants can no longer maintain stability through photoprotective or metabolic regulation,

29949890, 2026, 1, Downloaded from https://onlinelibrary.wiley.com/doi/10.1002/npp2.70038 by CochraneChina, Wiley Online Library on [08/06/2026]. See the Terms and Conditions (https://onlinelibrary.wiley.com/terms-and-conditions) on Wiley Online Library for rules of use; OA articles are governed by the applicable Creative Commons License

structural and efficiency related photosynthetic parameters tend to decline simultaneously.[48,49] The overall response pattern observed at this residue level in the present study is consistent with this general framework. From a hyperspectral perspective, pigment and canopy related indices exhibited broad and synchronous deterioration at 500 μg/kg. Chlorophyll-associated indices such as CHL3 declined markedly, accompanied by significant reductions in PRI and MTVI (Figure 2C,D,F), indicating impaired pigment status, reduced photosynthetic performance, and weakened canopy vitality. Previous work indicates that concurrent declines in chlorophyll indices and red edge parameters often reflect structural disruption of leaf internal organization[50] rather than reversible pigment adjustment. In the present study, both MCARI, MTVI, and MRENDVI reached their lowest values under high residue conditions (Figure 2C,F), supporting the interpretation that hyperspectral responses at this stage reflect structural degradation rather than adaptive modulation.

In addition, at the highest residual level of 500 μg/kg, several hyperspectral indices exhibited partial rebound responses relative to 100 μg/kg, including pigment- and structure-related indices (CHL1, CHL4, MCARI, and NDVI), stress and regulation related indices (NPQI and CRI2), as well as the water and light response index LRDSI (Figure 2C–F). Such non-monotonic behavior does not indicate recovery of physiological function, but is more likely attributable to non-linear relationships between spectral indices and actual physiological status under severe stress conditions. Previous studies have shown that under strong stress or substantial canopy structural damage, hyperspectral, and broadband vegetation indices may exhibit saturation, inverse responses, or reduced sensitivity to pigment content and photosynthetic performance, becoming increasingly influenced by residual canopy structure, spatial heterogeneity, pigment composition shifts, and altered optical pathways rather than linearly reflecting true physiological activity.[51] Accordingly, the rebound observed across CHL, MCARI, NDVI, NPQI, CRI2, and LRDSI based indices in the present study is more plausibly interpreted as an optical and signal-level response under advanced stress, rather than evidence of adaptive regulation or functional improvement.

UV-MCF fluorescence responses further distinguish this high-residue stage from the compensatory behavior observed at moderate exposure. Under sublethal stress conditions, increases in short-wavelength fluorescence (F450 and F542) have frequently been linked to the accumulation of phenolic compounds and enhanced stress-related metabolic activity (Figure 4A,B), serving as indicators of regulatory activation.[52] However, under more severe stress, such signals often fail to persist and may decrease as tissue integrity deteriorates. Consistent with this pattern, short-wavelength fluorescence in the present study did not show sustained increase at 500 μg/kg but instead declined. In contrast, chlorophyll-related emissions (F682 and F737) decreased sharply (Figure 4C,D). This transition from enhanced stress-related fluorescence to attenuated chlorophyll emission is indicative of a transition from regulatory compensation to functional failure, as photoprotective and metabolic adjustment can no longer sustain photosynthetic stability.[53] Chlorophyll fluorescence quenching parameters provide direct evidence of photosynthetic functional impairment at high residue levels. Numerous studies have shown that pronounced reductions in Fm (Figure 5A) and Fv/Fm (Figure 5B) indicate structural damage to PSII reaction centers, beyond the range of reversible regulation.[54–56] In the present study, both Fm_Lss and Fv/Fm_Lss declined substantially at 500 μg/kg, confirming severe impairment of PSII functionality. Although qP_Lss (Figure 5E) and QY_Lss (Figure 5F) increased at this concentration, these increases occurred in the context of strongly reduced maximum fluorescence and photochemical capacity, suggesting intensified utilization of a diminished pool of functional reaction centers rather than improved photosynthetic performance. Meanwhile, NPQ_Lss (Figure 5D) declined relative to its peak at moderate exposure, consistent with reports that photoprotective dissipation becomes constrained under extreme stress.[57] The concurrent decrease in Rfd_Lss (Figure 5C) further indicates a loss of assimilatory capacity at the system level.

At the integrative level, the transition from regulation to decline was captured by the sharp increase in the IBRv2 index (Figure 5G). Unlike the gradual elevation observed at lower and moderate residue levels, the abrupt rise in IBRv2 at 500 μg/kg reflects a simultaneous deviation in pigment status, energy regulation, and photochemical efficiency from control conditions. Similar abrupt increases in composite stress indices have been used to identify thresholds beyond which plant systems shift from compensatory adjustment to functional breakdown.[58] The present results further suggest that when a pronounced increase in IBRv2 coincides with declines in PSII structural parameters and a loss of coordinated regulatory responses, optical signals reflect a genuine functional deterioration rather than merely intensified regulation.

Overall, the optical response pattern observed under high residual nicosulfuron exposure aligns with previous descriptions of functional decline induced by severe non-photosynthetic-target herbicide stress.[59] By integrating hyperspectral, UV-MCF, and chlorophyll fluorescence evidence, this study refines the characterization of this transition and provides a clearer basis for distinguishing between regulation-dominated stress responses and the onset of functional phytotoxicity.

29949890, 2026, 1, Downloaded from https://onlinelibrary.wiley.com/doi/10.1002/npp2.70038 by CochraneChina, Wiley Online Library on [08/06/2026]. See the Terms and Conditions (https://onlinelibrary.wiley.com/terms-and-conditions) on Wiley Online Library for rules of use; OA articles are governed by the applicable Creative Commons License

4.5 | Linking functional optical responses with growth inhibition

The results of this study indicate that, under a well-defined residual dose gradient, soybean responses to nicosulfuron exhibit stage-dependent functional changes that precede and accompany growth inhibition. Growth-related traits such as emergence rate, plant height, and biomass effectively capture the final agronomic consequences of residual stress. However, these endpoints typically respond at relatively high residue levels. In contrast, multimodal optical indicators respond to dose variation at low to moderate residue levels, providing functional information on early and intermediate stress responses before pronounced growth suppression becomes evident.

By integrating hyperspectral reflectance, UV-MCF fluorescence, and chlorophyll fluorescence quenching parameters, this study demonstrates that residual nicosulfuron stress does not manifest as isolated optical signals but rather as coordinated functional responses across multiple optical dimensions along the dose gradient. Hyperspectral indices primarily reflect dose-dependent adjustments in pigment organization and canopy structure, UV-MCF fluorescence captures shifts in stress-related metabolic fluorescence and emission balance, and chlorophyll fluorescence parameters directly quantify changes in energy partitioning and photochemical efficiency. Together, these indicators exhibit coherent and ordered responses to increasing residue levels, reflecting an integrated reorganization of photosynthetic function under residual stress. In this framework, recovery potential is inferred not from a single parameter but from the coordination between regulatory and structural optical indicators. As long as regulatory responses (elevated NPQ_Lss, Rfd_Lss, and short wavelength fluorescence) remain active while structural PSII-related parameters (Fm_Lss and Fv/Fm_Lss) are not yet severely impaired, soybean seedlings are considered to retain functional adjustment capacity rather than having entered irreversible decline. At the mechanistic level, this coordinated optical behavior can be traced back to the primary biochemical action of nicosulfuron on acetolactate synthase (ALS), whose inhibition blocks the biosynthesis of branched-chain amino acids and initiates downstream metabolic imbalance.[60] Collectively, the results outline a coherent mechanistic pathway: nicosulfuron exposure—ALS inhibition—amino acid deficiency—oxidative stress—accumulation of secondary metabolites and reactive oxygen species—disruption of PSII–PSI energy balance—altered fluorescence signatures—phenotypic stress expression.

From an applied standpoint, linking functional optical responses with growth inhibition provides a coherent framework for interpreting the residual effects of herbicides across the dose gradient. Growth suppression clearly marks the establishment of injury, whereas coordinated optical responses characterize earlier functional states in which regulation remains active. By considering both growth endpoints and multimodal optical behavior, the progression from early functional disturbances to growth limiting injuries can be more clearly delineated.

More broadly, this framework is not limited to nicosulfuron or ALS-inhibiting herbicides. Residual stress imposed by other non-photosynthetic-target agrochemicals or environmental contaminants may similarly induce coordinated functional optical responses prior to or alongside growth inhibition. Therefore, embedding optical information within a dose response context offers a transferable approach for stage-specific interpretation of crop functional responses under residual stress.

5 | CONCLUSION

This study establishes an integrative optical approach that reveals how nicosulfuron induces a stepwise progression of photosynthetic impairment in soybean.

Soybean plants exposed to residual nicosulfuron exhibited significant physiological changes prior to the pronounced inhibition of growth. While reductions in emergence, plant height, and biomass mainly occurred at higher residue levels, alterations in hyperspectral reflectance, UV-induced fluorescence, and chlorophyll fluorescence parameters were already detectable even at low to moderate concentrations. These optical responses indicated early disturbances in pigment status, fluorescence emission balance, and photosynthetic energy regulation, which subsequently developed into measurable growth suppression.

By jointly evaluating multiple optical indicators, this study clarifies the progression of early physiological disruption towards growth limiting injury along a residue gradient. The results demonstrate that optical measurements can reveal functional stress in soybean seedlings at stages when conventional growth traits still appear largely unaffected. This approach provides a practical basis for identifying herbicide carryover effects earlier and more reliably than assessment based solely on growth metrics alone, and may be extended to evaluate residual stress caused by other non-photosynthetic-target agrochemicals in sensitive crops.

AUTHOR CONTRIBUTIONS

Shufei Hao: Software; methodology; writing—original draft; formal analysis; data curation. **Zekai Huang**: Formal analysis; investigation. **Olga A. Glazunova**: Formal analysis. **Konstantin V. Moiseenko**: Investigation. **Chi Wu**: Supervision; funding acquisition; project administration; writing—review and editing; validation. **Xingang Liu**: Supervision; funding acquisition;

29949890, 2026, 1, Downloaded from https://onlinelibrary.wiley.com/doi/10.1002/npp2.70038 by CochraneChina, Wiley Online Library on [08/06/2026]. See the Terms and Conditions (https://onlinelibrary.wiley.com/terms-and-conditions) on Wiley Online Library for rules of use; OA articles are governed by the applicable Creative Commons License

writing—review and editing; project administration; validation.

ACKNOWLEDGMENTS

We would like to thank Yuzhu Wang for his assistance with study conceptualization. We also thank Prof. Lan Zhang, Liangang Mao, and Lizhen Zhu for their valuable comments and suggestions that helped improve the manuscript. This work was financially supported by the National Key Research and Development Program of China (2023YFD1701300). National Key Research and Development Program of China (2024YFD1701101), and the project "Green Nano-Pesticides: Mechanisms of Reduction, Synergistic Efficiency, and Source-Controlled Pollution Mitigation" funded by the Basic Research Center, Innovation Program of Chinese Academy of Agricultural Sciences (Grant No. CAAS-BRC-GLCA-2025-01). We also thank the Beijing Ecotech Science and Technology Ltd. (Beijing, China) for providing technical and equipment support for the determination of photosynthesis indicators.

CONFLICT OF INTEREST STATEMENT

The authors declare no conflicts of interest.

DATA AVAILABILITY STATEMENT

The data that support the findings of this study are available on request from the corresponding author. The data are not publicly available due to privacy or ethical restrictions.

ORCID

Chi Wu https://orcid.org/0009-0009-0518-1940

REFERENCES

1. Parven, A., Meftaul, I. M., Venkateswarlu, K., & Megharaj, M. (2025). Herbicides in modern sustainable agriculture: Environmental fate, ecological implications, and human health concerns. *International Journal of Environmental Science and Technology*, *22*(2), 1181–1202. https://doi.org/10.1007/s13762-024-05818-y
2. Knuth, D., Gai, L., Silva, V., Harkes, P., Hofman, J., Šudoma, M., Bílková, Z., Alaoui, A., Mandrioli, D., Pasković, I., Polić Pasković, M., Baldi, I., Bureau, M., Alcon, F., Contreras, J., Glavan, M., Abrantes, N., Campos, I., Norgaard, T., … Geissen, V. (2024). Pesticide residues in organic and conventional agricultural soils across Europe: Measured and predicted concentrations. *Environmental Science & Technology*, *58*(15), 6744–6752. https://doi.org/10.1021/acs.est.3c09059
3. Yang, M., Wang, Y., Yang, G., Wang, Y., Liu, F., & Chen, C. (2024). A review of cumulative risk assessment of multiple pesticide residues in food: Current status, approaches and future perspectives. *Trends in Food Science and Technology*, *144*, 104340. https://doi.org/10.1016/j.tifs.2024.104340
4. Tang, T., Lei, C. T., Lv, L., Wang, F. D., Cheng, X., Gao, M. Y., Lou, J. J., Zhu, Y. K., Xu, N. H., Zhang, Q., Lu, T., & Qian, H. F. (2025). Systematic assessments of ecological and health risks of soil pesticide residues. *Environmental Pollution*, *375*, 126348. https://doi.org/10.1016/j.envpol.2025.126348
5. Virk, A. L., Shakoor, A., Ahmad, N., Du, H., Chang, S. X., & Cai, Y. (2025). Organic amendments restore soil biological properties under pesticides application. *Pesticide Biochemistry and Physiology*, *210*, 106394. https://doi.org/10.1016/j.pestbp.2025.106394
6. Fan, Q., Shen, Y., Yang, Y., & Zhang, Q. (2024). A review of remediation strategies for diphenyl ether herbicide contamination. *Toxics*, *12*(6), 397. https://doi.org/10.3390/toxics12060397
7. Jursík, M., Kolárová, M., & Kučera, J. (2025). Effect of residues of acetolactate synthase inhibiting herbicides in soil on oil-seed rape and sugar beet. *Crop Protection*, *197*, 107290. https://doi.org/10.1016/j.cropro.2025.107290
8. Manfo, F. P. T., Nimako, C., Nantia, E. A., Suh, C. F., Chenwi, S. P., Cho-Ngwa, F., Moundipa, P. F., Nakayama, S. M. M., Ishizuka, M., & Ikenaka, Y. (2024). Exposure of male farmers and nonfarmers to neonicotinoid pesticides in the South-West and Littoral Regions of Cameroon: A comparative study. *Environmental Toxicology and Chemistry*, *43*(5), 952–964. https://doi.org/10.1002/etc.5842
9. Grint, K. R., Proctor, C., DeWerff, R., Smith, D. H., Arneson, N. J., Arriaga, F., Stoltenberg, D., & Werle, R. (2022). Low carryover risk of corn and soybean herbicides across soil management practices and environments. *Weed Technology*, *36*(1), 160–167. https://doi.org/10.1017/wet.2021.97
10. Chen, F., Wu, C., Wang, Y., Glazunova, O. A., Moiseenko, K. V., Zhang, L., Mao, L., Zhu, L., & Liu, X. (2025). Phytotoxicity of fluridone and emerging transformation products in agricultural soils: Insights into molecular interactions and photosynthetic disruptions in maize. *Journal of Hazardous Materials*, *496*, 139252. https://doi.org/10.1016/j.jhazmat.2025.139252
11. Wu, C., Wang, Y., Clarke, J. L., Su, H., Wang, L., Glazunova, O. A., Moiseenko, K. V., Zhang, L., Mao, L., Zhu, L., & Liu, X. (2025). Biochar enhances the sorption and degradation of fluridone and its main metabolite in soil: Insights into biodegradation potential and remediation of microbial communities. *Biochar*, *7*(1), 81. https://doi.org/10.1007/s42773-025-00469-9
12. Zhao, B. C., Xu, X., Li, B. H., Qi, Z. Z., Huang, J. A., Hu, A. L., Wang, G. Q., & Liu, X. M. (2023). Target-site mutation and enhanced metabolism endow resistance to nicosulfuron in a Digitaria sanguinalis population. *Pesticide Biochemistry and Physiology*, *194*, 105488. https://doi.org/10.1016/j.pestbp.2023.105488
13. Choe, E., & Williams, M. M. (2020). Expression and comparison of sweet corn CYP81A9s in relation to nicosulfuron sensitivity. *Pest Management Science*, *76*(9), 3012–3019. https://doi.org/10.1002/ps.5848
14. Huang, Z., Huang, H., Chen, J., Chen, J., Wei, S., & Zhang, C. (2019). Nicosulfuron-resistant Amaranthus retroflexus L. in Northeast China. *Crop Protection*, *122*, 79–83. https://doi.org/10.1016/j.cropro.2019.04.024
15. Wright, T. R., Bascomb, N. F., Sturner, S. F., & Penner, D. (1998). Biochemical mechanism and molecular basis for ALS-inhibiting herbicide resistance in sugarbeet (Beta vulgaris) somatic cell selections. *Weed Science*, *46*(1), 13–23. https://doi.org/10.1017/S0043174500090111
16. Brown, L. R., Robinson, D. E., Young, B. G., Loux, M. M., Johnson, W. G., Nurse, R. E., Swanton, C. J., & Sikkema, P. H. (2009). Response of corn to simulated glyphosate drift followed by in-crop herbicides. *Weed Technology*, *23*(1), 11–16. https://doi.org/10.1614/WT-08-067.1
17. Wang, K., Ren, Y., Pan, X., Wu, X., Xu, J., Zheng, Y., & Dong, F. (2025). Insights on persistent herbicides in cropland soils in northern China: Occurrence, ecological risks, and phytotoxicity to subsequent crops. *Journal of Hazardous Materials*, *490*, 137794. https://doi.org/10.1016/j.jhazmat.2025.137794
18. Silva, A. F. M., Albrecht, A. J. P., Silva, G. S., Kashivaqui, E. S. F., Albrecht, L. P., & Victoria, R. (2019). Rates of nicosulfuron applied in glyphosate-tolerant and sulfonylurea-tolerant

29949890, 2026, 1, Downloaded from https://onlinelibrary.wiley.com/doi/10.1002/npp2.70038 by CochraneChina, Wiley Online Library on [08/06/2026]. See the Terms and Conditions (https://onlinelibrary.wiley.com/terms-and-conditions) on Wiley Online Library for rules of use; OA articles are governed by the applicable Creative Commons License

soybean. *Planta Daninha*, *37*, e0372019. https://doi.org/10.1590/S0100-83582019370100010
19. Brazier-Hicks, M., Franco-Ortega, S., Watson, P., Rougemont, B., Cohn, J., Dale, R., Hawkes, T. R., Goldberg-Cavalleri, A., Onkokesung, N., & Edwards, R. (2022). Characterization of cytochrome P450s with key roles in determining herbicide selectivity in maize. *ACS Omega*, *7*(20), 17416–17431. https://doi.org/10.1021/acsomega.2c01705
20. Bierman, A., LaPlumm, T., Cadle-Davidson, L., Gadoury, D., Martinez, D., Sapkota, S., & Rea, M. (2019). A high-throughput phenotyping system using machine vision to quantify severity of grapevine powdery mildew. *Plant Phenomics*, *2019*, 9209727. https://doi.org/10.34133/2019/9209727
21. Wang, J., Gao, H., Guo, Z. Q., Meng, Y. Y., Yang, M., Li, X. L., & Yang, Q. (2021). Adaptation responses in C4 photosynthesis of sweet maize (*Zea mays* L.) exposed to nicosulfuron. *Ecotoxicology and Environmental Safety*, *214*, 112096. https://doi.org/10.1016/j.ecoenv.2021.112096
22. Xiao, T., Yang, L., He, X., Wang, L., Zhang, D., Cui, T., Zhang, K., Li, H., Li, Z., & Dong, J. (2025). Assessing the ecotoxicological risk of nicosulfuron on maize using multi-source phenotype data and hyperspectral imaging. *Ecotoxicology and Environmental Safety*, *295*, 118176. https://doi.org/10.1016/j.ecoenv.2025.118176
23. Zhang, J. N., Feng, X. P., Wu, Q. G., Yang, G. F., Tao, M. Z., Yang, Y., & He, Y. (2022). Rice bacterial blight resistant cultivar selection based on visible/near-infrared spectrum and deep learning. *Plant Methods*, *18*(1), 49. https://doi.org/10.1186/s13007-022-00882-2
24. Rossini, M., Nedbal, L., Guanter, L., Ac, A., Alonso, L., Burkart, A., Cogliati, S., Colombo, R., Damm, A., Drusch, M., Hanus, J., Janoutova, R., Julitta, T., Kokkalis, P., Moreno, J., Novotny, J., Panigada, C., Pinto, F., Schickling, A., … Rascher, U. (2015). Red and far red Sun-induced chlorophyll fluorescence as a measure of plant photosynthesis. *Geophysical Research Letters*, *42*(6), 1632–1639. https://doi.org/10.1002/2014GL062943
25. Hu, Y., Ma, B., Wang, H., Li, Y., Zhang, Y., & Yu, G. (2023). Non-destructive detection of different pesticide residues on the surface of Hami melon classification based on tHBA-ELM algorithm and SWIR hyperspectral imaging. *Foods*, *12*(9), 1773. https://doi.org/10.3390/foods12091773
26. Wang, Z. M., Zheng, S., Wang, C. W., Zhang, L., Liu, Y., Wu, X. S., & Wang, S. (2024). A novel competitive color-tone change fluorescence immunochromatographic assay for the ultrasensitive detection of pesticide and veterinary drug residues. *Sensors and Actuators B: Chemical*, *417*, 136125. https://doi.org/10.1016/j.snb.2024.136125
27. Yang, Y., Nan, R., Mi, T., Song, Y., Shi, F., Liu, X., Wang, Y., Sun, F., Xi, Y., & Zhang, C. (2023). Rapid and nondestructive evaluation of wheat chlorophyll under drought stress using hyperspectral imaging. *International Journal of Molecular Sciences*, *24*(6), 5825. https://doi.org/10.3390/ijms24065825
28. Sanchez, W., Burgeot, T., & Porcher, J. M. (2013). A novel "Integrated Biomarker Response" calculation based on reference deviation concept. *Environmental Science and Pollution Research*, *20*(5), 2721–2725. https://doi.org/10.1007/s11356-012-1359-1
29. Beliaeff, B., & Burgeot, T. (2002). Integrated biomarker response: A useful tool for ecological risk assessment. *Environmental Toxicology and Chemistry*, *21*(6), 1316–1322. https://doi.org/10.1002/etc.5620210629
30. Wang, X., Sun, C., Gao, S., Wang, L., & Shuokui, H. (2001). Validation of germination rate and root elongation as indicator to assess phytotoxicity with *Cucumis sativus*. *Chemosphere*, *44*(8), 1711–1721. https://doi.org/10.1016/S0045-6535(00)00520-8
31. Main, R., Felix, M. J. B., Watt, M. S., & Hartley, R. J. L. (2025). Early detection of herbicide-induced tree stress using uav-based multispectral and hyperspectral imagery. *Forests*, *16*(8), 1240. https://doi.org/10.3390/f16081240
32. Zhao, D., Cao, Y., Li, J., Cao, Q., Li, J., Guo, F., Feng, S., & Xu, T. (2024). Early detection of rice leaf blast disease using unmanned aerial vehicle remote sensing: A novel approach integrating a new spectral vegetation index and machine learning. *Agronomy*, *14*(3), 602. https://doi.org/10.3390/agronomy14030602
33. Javornik, T., Carović-Stanko, K., Gunjača, J., Vidak, M., & Lazarević, B. (2023). Monitoring drought stress in common bean using chlorophyll fluorescence and multispectral imaging. *Plants*, *12*(6), 1386. https://doi.org/10.3390/plants12061386
34. Maimaitiyiming, M., Ghulam, A., Bozzolo, A., Wilkins, J. L., & Kwasniewski, M. T. (2017). Early detection of plant physiological responses to different levels of water stress using reflectance spectroscopy. *Remote Sensing*, *9*(7), 745. https://doi.org/10.3390/rs9070745
35. Blackburn, G. A. (2007). Hyperspectral remote sensing of plant pigments. *Journal of Experimental Botany*, *58*(4), 855–867. https://doi.org/10.1093/jxb/erl123
36. Kalaji, H. M., Carpentier, R., Allakhverdiev, S. I., & Bosa, K. (2012). Fluorescence parameters as early indicators of light stress in barley. *Journal of Photochemistry and Photobiology B: Biology*, *112*, 1–6. https://doi.org/10.1016/j.jphotobiol.2012.03.009
37. Stefanov, M., Rashkov, G., Borisova, P., & Apostolova, E. (2023). Sensitivity of the photosynthetic apparatus in maize and sorghum under different drought levels. *Plants*, *12*(9), 1863. https://doi.org/10.3390/plants12091863
38. Agathokleous, E. (2021). The rise and fall of photosynthesis: Hormetic dose response in plants. *Journal of Forestry Research*, *32*(2), 889–898. https://doi.org/10.1007/s11676-020-01252-1
39. Wiedman, S., & Appleby, A. (2006). Plant growth stimulation by sublethal concentrations of herbicides. *Weed Research*, *12*(1), 65–74. https://doi.org/10.1111/j.1365-3180.1972.tb01188.x
40. Vukadinović, L., Galić, V., Brkić, A., Jambrović, A., & Šimić, D. (2025). Comparing chlorophyll fluorescence and hyperspectral indices in drought-stressed young plants in a maize diversity panel. *Agronomy*, *15*(7), 1604. https://doi.org/10.3390/agronomy15071604
41. Mohamed, E., Tomimatsu, H., & Hikosaka, K. (2025). The relationships between photochemical reflectance index (PRI) and photosynthetic status in radish species differing in salinity tolerance. *Journal of Plant Research*, *138*(2), 231–241. https://doi.org/10.1007/s10265-025-01615-x
42. Lee Jones, A., Ormondroyd, A., Hayes, F., & Jeffers, E. S. (2024). Reflections of stress: Ozone damage in broadleaf saplings can be identified from hyperspectral leaf reflectance. *Environmental Pollution*, *360*, 124642. https://doi.org/10.1016/j.envpol.2024.124642
43. Manley, P. V., Sagan, V., Fritschi, F. B., & Burken, J. G. (2019). Remote sensing of explosives-induced stress in plants: Hyperspectral imaging analysis for remote detection of unexploded threats. *Remote Sensing*, *11*(15), 1827. https://doi.org/10.3390/rs11151827
44. Clevers, J., & Kooistra, L. (2012). Using hyperspectral remote sensing data for retrieving canopy chlorophyll and nitrogen content. *Ieee Journal of Selected Topics in Applied Earth Observations and Remote Sensing*, *5*(2), 574–583. https://doi.org/10.1109/jstars.2011.2176468
45. Tian, Y., Xie, L., Wu, M., Yang, B., Ishimwe, C., Ye, D., & Weng, H. (2021). Multicolor fluorescence imaging for the early detection of salt stress in *Arabidopsis*. *Agronomy*, *11*(12), 2577. https://doi.org/10.3390/agronomy11122577
46. Murchie, E. H., & Ruban, A. V. (2020). Dynamic non-photochemical quenching in plants: From molecular mechanism to productivity. *The Plant Journal*, *101*(4), 885–896. https://doi.org/10.1111/tpj.14601

29949890, 2026, 1, Downloaded from https://onlinelibrary.wiley.com/doi/10.1002/npp2.70038 by CochraneChina, Wiley Online Library on [08/06/2026]. See the Terms and Conditions (https://onlinelibrary.wiley.com/terms-and-conditions) on Wiley Online Library for rules of use; OA articles are governed by the applicable Creative Commons License

47. Stefanov, M. A., Rashkov, G. D., & Apostolova, E. L. (2022). Assessment of the photosynthetic apparatus functions by chlorophyll fluorescence and P_{700} absorbance in C3 and C4 plants under physiological conditions and under salt stress. *International Journal of Molecular Sciences*, *23*(7), 3768. https://doi.org/10.3390/ijms23073768
48. Didaran, F., Kordrostami, M., Ghasemi-Soloklui, A. A., Pashkovskiy, P., Kreslavski, V., Kuznetsov, V., & Allakhverdiev, S. I. (2024). The mechanisms of photoinhibition and repair in plants under high light conditions and interplay with abiotic stressors. *Journal of Photochemistry and Photobiology B: Biology*, *259*, 113004. https://doi.org/10.1016/j.jphotobiol.2024.113004
49. Sharma, N., Nagar, S., Thakur, M., Suriyakumar, P., Kataria, S., Shanker, A. K., Landi, M., & Anand, A. (2023). Photosystems under high light stress: Throwing light on mechanism and adaptation. *Photosynthetica*, *61*(2), 250–263. https://doi.org/10.32615/ps.2023.021
50. Neuwirthová, E., Lhotáková, Z., & Albrechtová, J. (2017). The effect of leaf stacking on leaf reflectance and vegetation indices measured by contact probe during the season. *Sensors*, *17*(6), 1202. https://doi.org/10.3390/s17061202
51. Tian, Z., Fan, J., Yu, T., de Leon, N., Kaeppler, S. M., & Zhang, Z. (2025). Mitigating NDVI saturation in imagery of dense and healthy vegetation. *ISPRS Journal of Photogrammetry and Remote Sensing*, *227*, 234–250. https://doi.org/10.1016/j.isprsjprs.2025.06.013
52. Gawlik-Dziki, U., Wrzesińska-Krupa, B., Nowak, R., Pietrzak, W., Zyprych-Walczak, J., & Obrępalska-Stęplowska, A. (2023). Herbicide resistance status impacts the profile of non-anthocyanin polyphenolics and some phytomedical properties of edible cornflower (*Centaurea cyanus* L.) flowers. *Scientific Reports*, *13*(1), 11538. https://doi.org/10.1038/s41598-023-38520-z
53. Ruban, A. V. (2016). Nonphotochemical chlorophyll fluorescence quenching: Mechanism and effectiveness in protecting plants from photodamage. *Plant Physiology*, *170*(4), 1903–1916. https://doi.org/10.1104/pp.15.01935
54. Baker, N., & Oxborough, K. (2004). Chlorophyll fluorescence as a probe of photosynthetic productivity. In G. C. Papageorgiou & Govindjee (Eds.), *Chlorophyll a fluorescence. advances in photosynthesis and respiration* (Vol. *19*, pp. 65–82). Springer. https://doi.org/10.1007/978-1-4020-3218-9_3
55. Maxwell, K., & Johnson, G. N. (2000). Chlorophyll fluorescence—A practical guide. *Journal of Experimental Botany*, *51*(345), 659–668. https://doi.org/10.1093/jexbot/51.345.659
56. Murchie, E. H., & Lawson, T. (2013). Chlorophyll fluorescence analysis: A guide to good practice and understanding some new applications. *Journal of Experimental Botany*, *64*(13), 3983–3998. https://doi.org/10.1093/jxb/ert208
57. Jiao, Q., & Hu, X. (2025). Recent advances and emerging trends in chlorophyll fluorescence parameter Fv/Fm. *Phyton-International Journal of Experimental Botany*, *94*(9), 2615–2630. https://doi.org/10.32604/phyton.2025.069246
58. Catteau, A., Le Guernic, A., Palos Ladeiro, M., Dedourge-Geffard, O., Bonnard, M., Bonnard, I., Delahaut, L., Bado-Nilles, A., Porcher, J. M., Lopes, C., Geffard, O., & Geffard, A. (2023). Integrative biomarker response-Threshold (IBR-T): Refinement of IBRv2 to consider the reference and threshold values of biomarkers. *Journal of Environmental Management*, *341*, 118049. https://doi.org/10.1016/j.jenvman.2023.118049
59. Eceiza, M. V., Barco-Antoñanzas, M., Gil-Monreal, M., Huybrechts, M., Zabalza, A., Cuypers, A., & Royuela, M. (2022). Role of oxidative stress in the physiology of sensitive and resistant Amaranthus palmeri populations treated with herbicides inhibiting acetolactate synthase. *Frontiers in Plant Science*, *13*, 1040456. https://doi.org/10.3389/fpls.2022.1040456
60. Kwon, C. S., & Penner, D. (1995). Response of a chlorsulfuron-resistant biotype of *Kochia scoparia* to ALS inhibiting herbicides and piperonyl butoxide. *Weed Science*, *43*(4), 561–565. https://doi.org/10.1017/S0043174500081649

SUPPORTING INFORMATION

Additional supporting information can be found online in the Supporting Information section at the end of this article.

29949890, 2026, 1, Downloaded from https://onlinelibrary.wiley.com/doi/10.1002/npp2.70038 by CochraneChina, Wiley Online Library on [08/06/2026]. See the Terms and Conditions (https://onlinelibrary.wiley.com/terms-and-conditions) on Wiley Online Library for rules of use; OA articles are governed by the applicable Creative Commons License